Carbon 152 (2019) 503–510

Contents lists available at ScienceDirect

Carbon

journal homepage: www.elsevier.com/locate/carbon

Electrodeposition behavior of lithium metal on carbon substrates with surface silvering

Ran Tian [a], Ronghan Chen [b], Zhenming Xu [b], Songlin Wan [a], Lin Guan [a], Huanan Duan [a, *], Hua Li [a], Hong Zhu [b], Di Sun [c], Hezhou Liu [a, **]

[a] State Key Laboratory of Metal Matrix Composites, School of Materials Science and Engineering, Shanghai Jiao Tong University, Shanghai, 200240, PR China
[b] University of Michigan – Shanghai Jiao Tong University Joint Institute, Shanghai Jiao Tong University, Shanghai, 200240, PR China
[c] Department of Ultrasound in Medicine, Shanghai Jiao Tong University Affiliated Sixth People's Hospital, Shanghai Institute of Ultrasound in Medicine, Shanghai, 200233, PR China

ARTICLE INFO

Article history:
Received 15 April 2019
Received in revised form
14 June 2019
Accepted 15 June 2019
Available online 17 June 2019

Keywords:
Lithium metal anode
Carbon substrates
Electrodeposition
Surface silvering

ABSTRACT

Li-ion batteries (LIBs), the widely used energy storage devices, have been intensively studied to further increase their energy density and working life. To this end, lithium metal is the most promising high-capacity anode material, but the unstable electrochemical performance and dendrites formation inhibit its development. Based on DFT calculation, the adsorption energy analysis shows that the preferential and uniform Li deposition may occur on Li–Ag surface comparing to bare carbon surface. Therefore, we adopt thermal evaporation to silver the carbon surface to change the electrodeposition behavior of lithium metal. Li metal preferentially deposits on the Ag surface with flat appearance, restraining the formation of Li dendrites. The lithium metal/carbon composite anodes are subsequently prepared by electrodepositing Li metal on the bare or the modified carbon substrates, and three types of cell configurations, namely, Ag (B), bare CP and Ag (F), are compared in terms of electrochemical performance. The results show that the Ag (B) cell can effectively prolong the short-circuit time, enhance the electrochemical stability in the Coulombic efficiency, and better retain the specific capacity in full-cell tests due to the suppression of "dead Li". This research provides a basic guidance for the electrochemical preparation of lithium metal/carbon composite anodes.

© 2019 Elsevier Ltd. All rights reserved.

1. Introduction

Nowadays, the development of consumer electronics and electric vehicles needs energy storage devices with higher energy/power densities more than ever. Among the candidate systems, lithium metal batteries that use lithium metal as anode materials have attracted the researchers' attention [1,2]. With the high theoretical specific capacity of 3860 mAh g^{-1} and the lowest electrochemical potential, lithium metal batteries such as Li–S and Li–O_2 systems could significantly increase the energy density compared with commercial Li-ion batteries (LIBs) [3–7]. But now, lithium metal batteries have not been employed on a large scale due to the inferior electrochemical stability. The main reason is the formation of lithium dendrites, which may cause solid electrolyte interface (SEI) layer fractures and infinite volume change [3,8–10]. Besides, the spiny structure raises the possibility of the separator penetration and thermal runaway. Up to now, a few methods have been proposed such as electrolyte optimization [11–13] and artificial interlayer [14–18] to improve the electrochemical performance of lithium metal. But an ultimate solution is not available yet.

Recently, the lithium metal/carbon composite material is an emerging solution for lithium metal anodes [14,19–26]. The carbon substrate can provide a conductive and steady scaffold for lithium metal. As an example, Cui and his co-workers designed a layered Li–rGO composite used as a Li metal anode [14]. The composite was prepared by infusing molten Li into lithiophilic interlayer spacing of the rGO. The anode exhibits stable cyclic performance with low hysteresis and a small electrode dimensional change (~20%) during cycling with stable SEI layer. However, the heat fusion method needs extremely inert atmosphere and is difficult for practical use. Therefore, Zhang et al. invented the electrochemical deposition

* Corresponding author.
** Corresponding author.
E-mail addresses: hd1@sjtu.edu.cn (H. Duan), hzhliu@sjtu.edu.cn (H. Liu).

https://doi.org/10.1016/j.carbon.2019.06.067
0008-6223/© 2019 Elsevier Ltd. All rights reserved.

process to synthesize lithium metal/carbon composite anodes [27]. They used nitrogen-doped graphene as the Li plating matrix to regulate Li metal nucleation and suppress dendrite growth. The graphene modified Li metal anode demonstrates a high Coulombic efficiency of 98% for near 200 cycles without lithium-dendrite generation.

The carbon cloth and carbon paper are common free-standing electrode materials in electrochemical devices [28–31], but their graphite structure is not suitable for over-lithiation and leads lithium-dendrite growth [21,32]. The lithium dendrites may cause "dead Li" formation and decrease the capacity of the cell [33,34]. As a result, they are not suitable for depositing much lithium metal to make the lithium metal/carbon composite anodes.

Herein, we develop a surface silvering method to change the lithium metal deposition behavior on carbon substrates. Using first principles modeling, we find the Li–Ag alloy has a lower surface over-lithiation energy than LiC_6 so that Li metal preferentially grows on the Li–Ag alloy. Afterwards, we prepare the lithium metal/carbon composite anodes with different Li metal deposition directions by different silvering surfaces. The Li metal deposited on the Ag surface has the tiled structure instead of dendrites. The electrochemical tests show that the composite electrode whose Ag surface is back to the separator can effectively prolong the short-circuit time, enhance the electrochemical stability in the Coulombic efficiency, and better retain the specific capacity in full-cell tests due to the suppression of "dead Li".

2. Experimental section

2.1. Surface modification of carbon substrate

Carbon cloth (denoted as CC, WOS1009, Cetech Co, Ltd) and Carbon paper (denoted as CP, TGP-H-060, TORAY) were chosen as the substrates to deposit thin silver film by thermal evaporation. The thermal evaporation was performed in vacuum to realize 20 nm deposition.

2.2. Lithium metal deposition on modified CP and short-circuit time (SCT) test

We used modified CP as the substrate to deposit lithium metal as the working electrode. The lithium metal (250 μm, MTI) was chosen as the reference and counter electrode to supply lithium. CR2025-type coin cells were assembled using the two electrodes, Celgard 2325 membrane, and 120 μL of conventional electrolyte 1 M LiTFSI in DOL/DME with 1% $LiNO_3$ (Shanghai Xiaoneng Corp.) in an Ar-filled glovebox. The deposition test was carried out by a galvanostatic process with LAND CT2001A battery testers. The current density was 0.2 mA cm^{-2} and the deposited capacity was 5 mAh cm^{-2}.

2.3. Lithium metal deposition on modified CC and Coulombic efficiency (CE) test

The deposition test for the CC was carried out with the same method as above except the electrolyte. The electrolyte was 1.0 M $LiPF_6$ in a mixture of ethylene carbonate, dimethyl carbonate, and ethyl methyl carbonate (volume ratio of 1:1:1, Shanshan Corp) with 2% fluoroethylene carbonate (FEC). The deposition test was carried out by a galvanostatic process with LAND CT2001A battery testers. The current density was 0.2 mA cm^{-2} and the deposited capacity was 5 mAh cm^{-2}. Electrochemical impedance spectra (EIS) measurements were carried out by using the Bio-logic VMP-3 electrochemical workstation from 100.0 KHz to 0.1 Hz with a potential interval of 5 mV.

2.4. Short-circuit time (SCT) test

The cells were constituted by the modified CP and Li metal electrodes. We took a 100 μm thick ring-shaped spacer instead of the polymer separator to test the SCT. The cell was measured with a 0.5 mA cm^{-2} galvanostatic discharge process. The time when the sharp change in the voltage-time profile occurred was identified as the SCT.

2.5. Coulombic efficiency (CE) test

The CE test was taken with the same coin cell with it in 2.3. We used the galvanostatic discharge/charge process with the specific capacity of 5 mAh cm^{-2} at the current density of 0.2 mA cm^{-2} for the first cycle and 1 mA cm^{-2} for the following cycles.

2.6. Full cell test

The full cells were constituted by the modified CC anodes with a 2 mAh cm^{-2} pre-lithiation and $LiCoO_2$ cathodes. $LiCoO_2$ (LCO) electrodes were fabricated with a standard slurry process (provided by Shanghai Xiaoneng Tech.). LCO, super P and PVDF were mixed in the weight ratio of 94:3:3 for slurry preparation. The slurry was spread on an Al foil with a loading mass of about 14.7 mg cm^{-2}. The electrolyte and separator were the same as those of the cells in the CE test. The galvanostatic cycling test was carried out with a LAND CT2001A cell tester at a current density of 0.2 mA cm^{-2} for the first cycle and 1.0 mA cm^{-2} for the following cycles in a voltage range of 4.25 to 2.7 V.

2.7. Materials characterization

The cycled electrodes were washed thoroughly by electrolytic solvent and dried at 70 °C in the glove-box for morphology characterization. The SEM images were taken on a TESCAN VEGA3 scanning electron microscopy.

2.8. DFT calculation

Our density functional theory (DFT) calculations were performed by using the Vienna *Ab initio* Simulation Package (VASP) [35] within the projector-augmented wave (PAW) approach [36]. The Perdew–Burke–Ernzerhof (PBE) generalized gradient approximations (GGA) [37] functions were used. To model the surface of Li–Ag (100) and LiC_6 (001), we created slabs with nine and seven atomic layers, respectively, both with 15 Å vacuum along the z direction. A 4×4 lateral cell for Li–Ag and a 3×3 one for LiC_6 were applied to achieve similar surface areas. Energy cutoff for plane-wave basis was 520 eV for all calculations. The convergence criteria for structural optimization were 0.1 eV $Å^{-1}$ in force, and 10^{-4} eV for the electronic step. The Brillouin zones were sampled with $3 \times 3 \times 1$ k points for both slabs.

We considered the Li adsorption energy ΔE as the descriptor of binding strengths of Li to surfaces. The adsorption energy was defined as $\Delta E = E_{ads} - E_{cleab} - E_{Li}$, where E_{ads}, E_{clean}, E_{Li} represented the DFT energy of Li-adsorbed slab, clean slab and single Li atom, respectively. According to this definition, a more negative adsorption energy indicated a more favorable lithiation reaction.

3. Results and discussion

3.1. DFT calculations for the lithium metal deposition on the carbon-based surface

To simulate the initial condition of lithium atoms on the carbon-

based substrate, we constructed the fully lithiated surface to deposit lithium atoms. On the Ag surface, Ag is lithiated to Li-Ag [38,39] alloy with the body-centered cubic structure. Therefore, we chose the (100) surface of Li–Ag alloy because of the lowest surface energy. As shown in Fig. 1, the adsorption energy of a Li atom on the Ag layer is −0.58 eV. Afterwards, the Li atoms fulfill the (100) surface so that it displays a monolayer of Li atoms. The energy for the adsorption of Li to Li monolayer increases significantly to 0.40 eV. This phenomenon reveals that the Li atom prefers to deposit on the Ag layer rather than the Li layer, which corresponds to the smooth Li metal deposition on the Ag surface. After that, we probed the condition for the graphite carbon. The layered LiC_6 compound is structured to represent the fully lithiated graphite [40]. The free surface is the (100) terminated by carbon atoms, the adsorption energy of Li atom on which is 0.53 eV, indicating the difficulty to over-lithiate LiC_6 to form LiC_3. On the contrary, the adsorption energy decreases to 0.12 eV if a Li atom deposits on the Li monolayer. The lower adsorption energy shows that the Li atom preferentially deposits on the Li metal surface and causes the lithium-dendrite formation on the over-lithiated graphite.

To determine the deposition order of Li metal on the modified carbon substrates, we compared the adsorption energies of the two surface conditions. The high adsorption energy on graphite terminated LiC_6 sets a big barrier for the metallic-Li deposition. The energy hill prevents the initial nucleation process, even though the energy decreases to 0.12 eV for the further deposition of Li to Li monolayer. Therefore, the lithium metal will preferentially deposit on the Ag surface on the carbon substrates, which means that the surface silvering can effectively alter the deposition behavior of metallic Li.

3.2. Ag thin-film on the carbon-based surface

From the foregoing calculated results, Ag is an effective alloy source to alter Li metal deposition behavior. So we took a thermal evaporation method to deposit 20-nm thick Ag film on the carbon substrates [41]. Because of the directionality of thermal evaporation, the Ag film was only present on the surface facing to the Ag source so that both sides of the substrate have very different surface properties. As shown in Fig. 2A, different sides of the modified CP show different colors. The left metallic sheen surface corresponds to the side facing the evaporator source while the black one is the back side. Thus, we call the two surfaces as Ag side and carbon side. In the SEM images of the two surfaces (Fig. 2B and C), there are mainly carbon fibers (diameter ~10 μm) without massive Ag particles. The SEM-EDS mapping (Fig. 2D–H) indicates that the Ag is distributed all over the carbon fibers on the Ag side. On the contrary, there is little Ag on the carbon side (Fig. S1). Similarly, the two surfaces of modified CC substrates exhibit very different element distribution (Figs. S2–4). The different surface properties provide an opportunity to study the electrodeposition behavior of lithium metal.

3.3. Lithium metal electrodeposition

The Ag thermal evaporation provides different surface properties of the CP electrode, on which we designed the lithium metal deposition experiment (Fig. 3). The cells were constituted by the lithium metal and CP electrodes. During the coin-cell assembly, we arranged the Ag side or the carbon side facing the lithium metal and defined the cells as “Ag (F)” or “Ag (B)” cells (Fig. 3A). Moreover, the cells with bare carbon paper and lithium metal were employed as control samples and named as “bare CP”. To explore the lithium metal deposition behavior of the three-cell types, we used the galvanostatic discharge process with the capacity of 5 mAh cm^{-2} in the ether-based electrolyte and then disassembled the cell to analyze the morphology of the electrodes. In the digital pictures of the electrodes after 5 mAh cm^{-2} deposition (Fig. 3B–G), the carbon side (face to the Li metal) of Ag (B) (Fig. 3B) turns to be yellowish due to the LiC_6 formation [42]. The silver area (highlighted in red circles) that sporadically spread on the surface are the lithium dendrites. The amount of lithium dendrites is much more on the

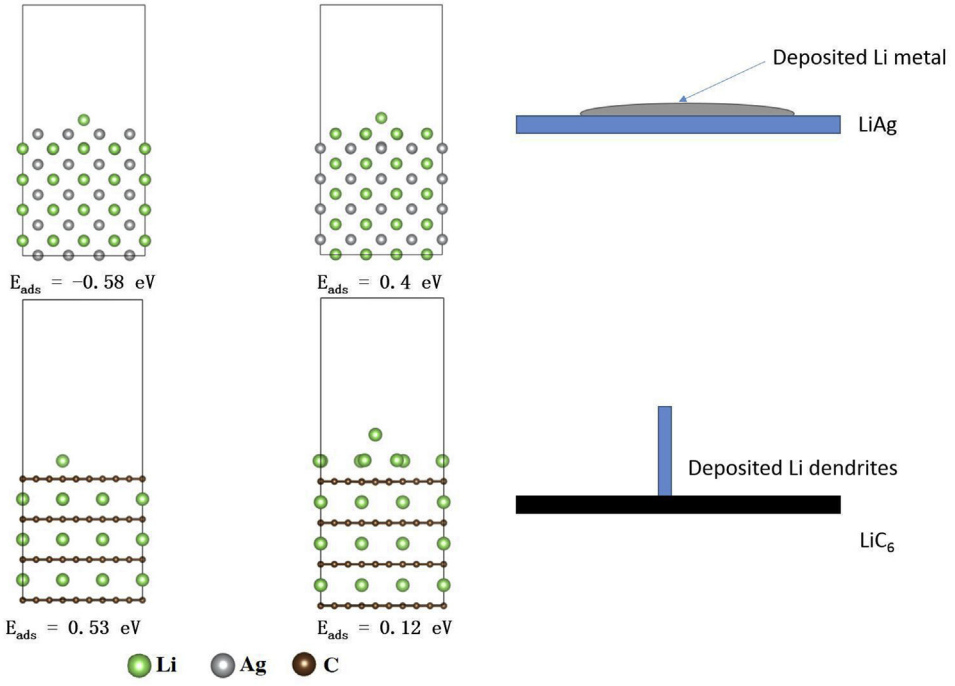

Fig. 1. DFT calculation results and schematics for adsorption of Li atoms on the Li–Ag and LiC_6 surfaces. (A colour version of this figure can be viewed online.)

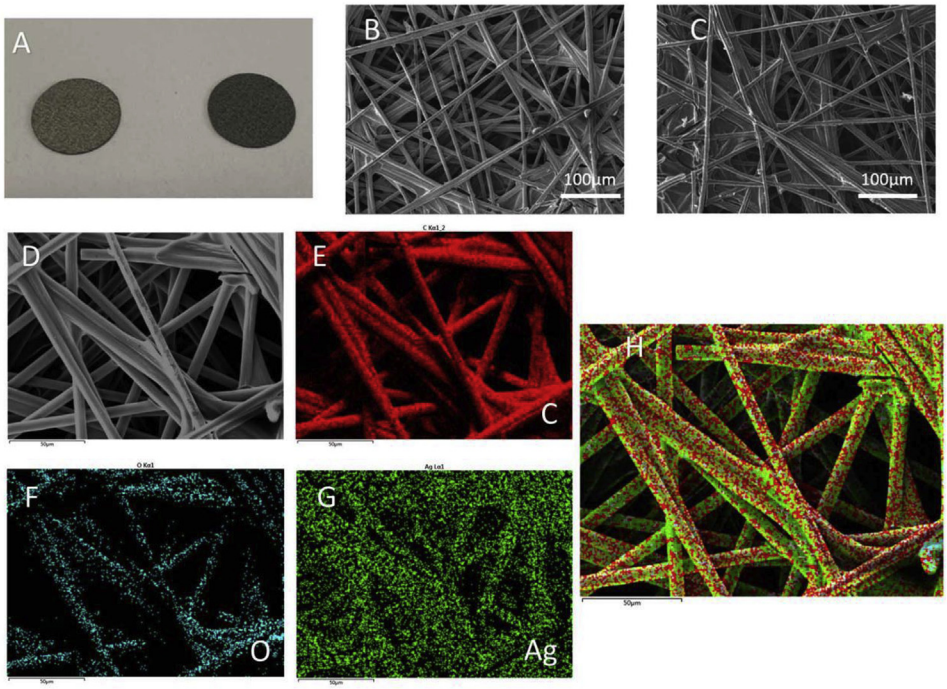

Fig. 2. Digital photo of the Ag modified carbon paper (A). SEM images of the Ag side (B) and carbon side (C) of the carbon paper. SEM-EDS-mapping (D–H) of the Ag side of the carbon paper. (A colour version of this figure can be viewed online.)

reverse Ag side (Fig. 3C), which indicates that Li metal is preferentially deposited on the Ag surface, consistent with the calculation results in Fig. 1. The bare CP electrode shows dense granular Li metal on the side facing Li metal and sparse granules on the back one (Fig. 3D and E). In Fig. 3F and G, the Ag (F) electrode exhibits the single-side deposition of Li metal on the Ag face (face to the Li metal).

The morphology of the electrodeposited Li metal was further studied by SEM. The surface status of Ag (B) electrode is shown in Fig. 4A and B. Obviously, there are sparse and vimineous Li dendrites on the carbon side (face to the Li metal); the Ag side (back to the Li metal) has granular and nodule-like Li metal. On contrast, Fig. 4C and D displays that Li dendrites on the surface of bare CP electrodes have a fluffy structure and the amount of the dendrites on the surface facing the Li metal is larger than that on the back one. Therefore, Li metal prefers to nucleate and grow on the surface with short diffusion path, but the silvered surface can effectively inhibit this trend. For the Ag (F) electrode (Fig. 4E and F), the metallic Li is mainly deposited on the Ag face (face to the Li metal). The densely deposited Li metal proves that the alloy-modified surface alters the growth behavior of Li metal.

To further study the electrodeposition behavior, we chose another carbon substrate, CC, and ester-based electrolyte to do similar galvanostatic tests. The digital images (Fig. S5) of the three CC samples are analogous to those of the CP above, which confirms that silvering can change the deposition order of Li metal on carbon surfaces. It is notable that the lithiated CC looks black rather than yellowish as CP, which results from the hybrid texture of layer-structured graphite and unorganized carbon in CC [20]. SEM images (Fig. S6) also show that in contrast to the carbon side in the surface-modified electrode, the metallic Li is mainly deposited on the Ag side. In addition, the ester-based electrolyte with the FEC additive gives the different Li metal morphology than the ether-based electrolyte. The metallic Li on the Ag side lies between the carbon fibers and is well compatible with silver surface. On

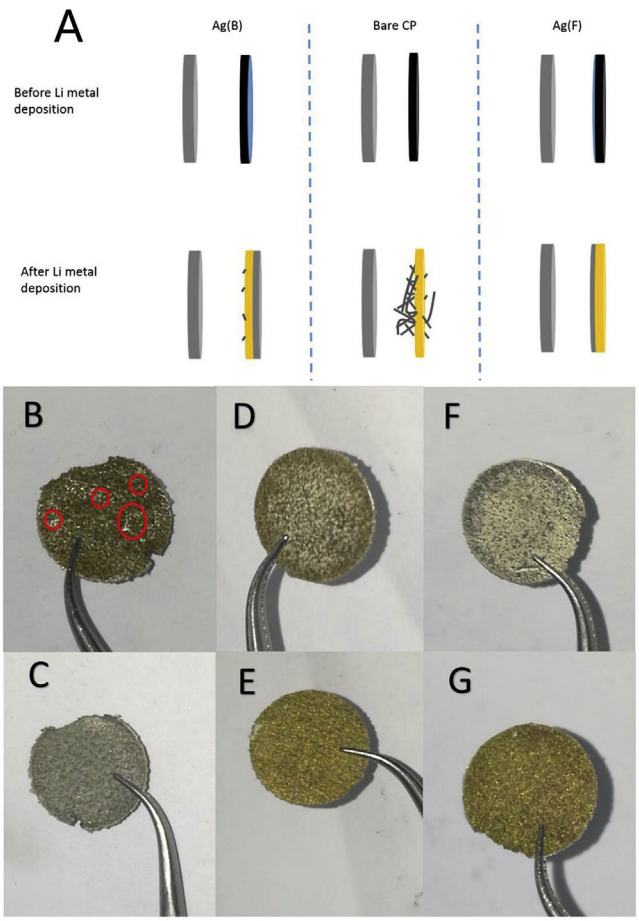

Fig. 3. The schematics of the deposition process (A). Digital photos of the surfaces in the Ag (B) cells (B and C), bare CP cells (D and E) and Ag (F) cells (F and G) after 5 mAh cm^{-2} discharge. (A colour version of this figure can be viewed online.)

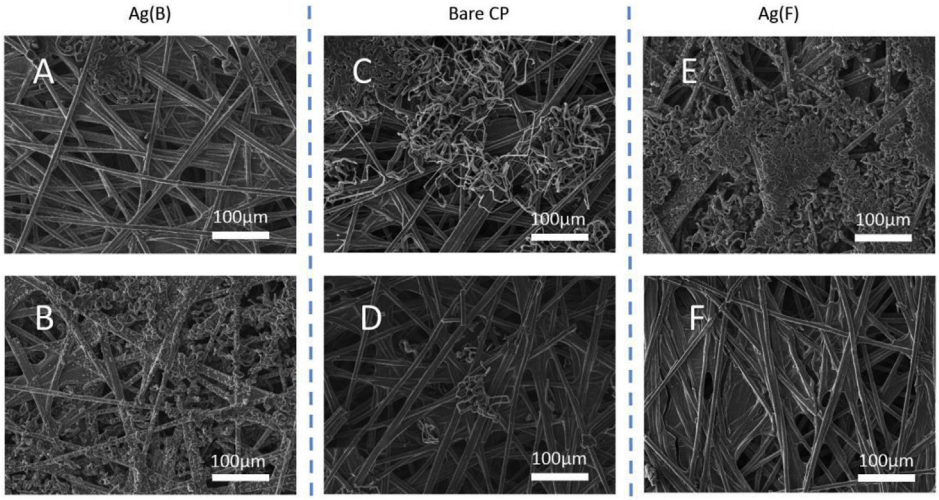

Fig. 4. SEM images of the surfaces in the Ag (B) cells (A, B), bare CP cells (C and D) and Ag (F) cells (E and F) after 5 mAh cm^{-2} discharge. (A colour version of this figure can be viewed online.)

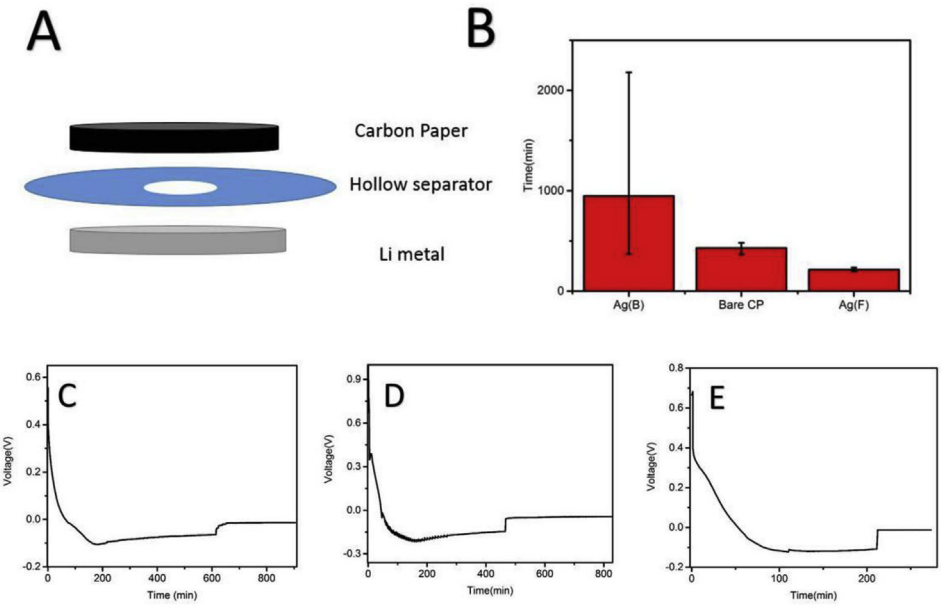

Fig. 5. Schematic of the battery for SCT tests (A). SCT time (B) and voltage-time curves for the Ag (B) (C), bare CP (D) and Ag (F) (E) cells. (A colour version of this figure can be viewed online.)

contrary, the Li metal on the carbon side is loosely attached to the carbon electrode, showing plate-like structure. This phenomenon demonstrates the lithophobiclity between CC and Li metal.

EIS measurement is an effective way to understand electrochemical property of the Li metal/carbon composite anode. The Nyquist plots of three Li metal/CC composite anodes after 5 mAh cm^{-2} discharge are displayed in Fig. S7. The semicircle occurring in the high-middle frequency region is attributed to the transfer resistance [43]. The Ag (F) cell exhibits obviously higher resistance because the dense Li metal layer provides fewer deposition sites. After fitting the profiles by Z-Fit (Fig. S8 and Table S1), the R_{total} of Ag (B) is 34.195 Ω, which is close to the 35.306 Ω of bare CC.

In short, the silvered surface can affect the electrodeposition order and morphology of Li metal on various carbon-based substrates in both ester-based and ether-based electrolytes. It provides a potential way to prepare Li metal/carbon composite anodes with controlled Li metal locations.

3.4. SCT tests of the composite anodes

The unique structure of the Li metal/carbon composite anodes may lead to advantageous applications in the cell. The direction of Li metal deposition on the silvered carbon substrates in Ag (B) cells is away from the separator, which might help prevent separator penetration. Therefore, we adopted the SCT test to study this effect [44,45]. Because of the high mechanical property of the commercial separator, a hollow separator ring was used to expedite the SCT test (Fig. 5A) [44,46]. The inner diameter of the hole is 6 mm, and the thickness of the paper is 0.1 mm (Fig. S9). Because the high roughness of CC may cause uncontrolled short-circuit, we used the

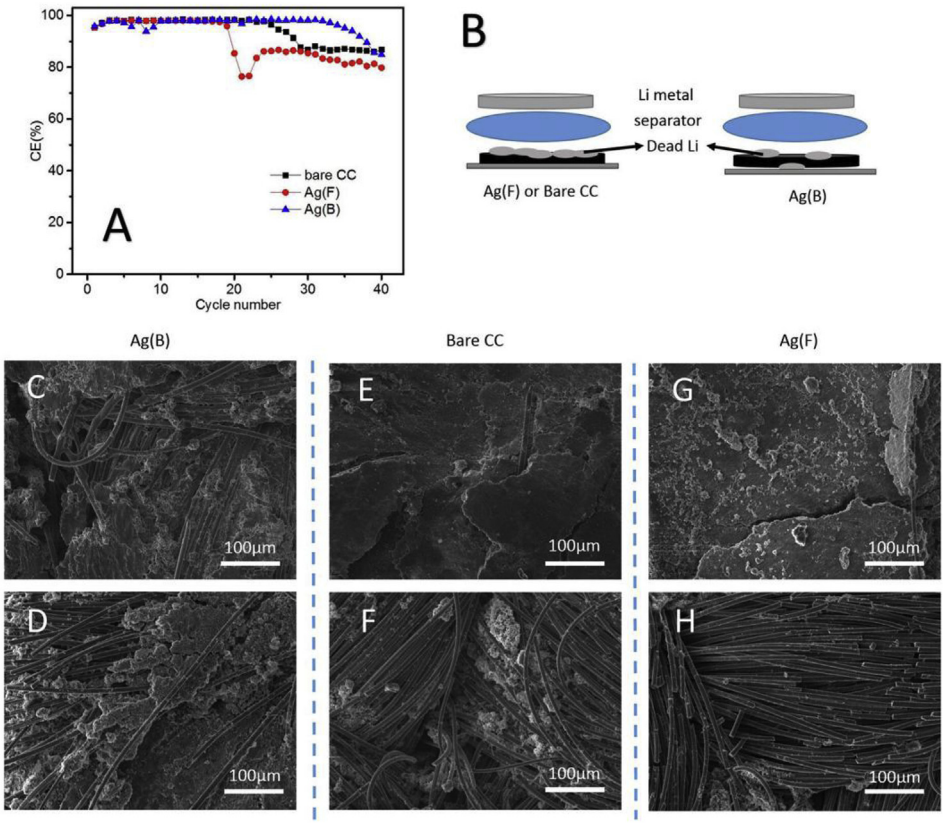

Fig. 6. CEs (A) and schematic (B) for the CE tests. SEM images of the surfaces in the Ag (B) cells (C and D), bare CC cells (E and F) and Ag (F) cells (G and H) after 40 cycles. (A colour version of this figure can be viewed online.)

modified CP as the test groups. During the 0.5 mA cm^{-2} galvanostatic discharge process, the Li is continuously stripped from the Li counter electrode and plated on the CP electrodes until the battery fails (Fig. 5A) [45]. By recording the voltage profile against the time, the point at which the voltage drastically changes is the value of SCT. SCT can quantitatively describe the Li dendrite formation process and the safety of the Li metal/carbon composite anodes.

As shown in Figure 5C-E, the voltage-time profiles look similar for the three types of cells, namely, Ag (B), bare CP and Ag (F). At the beginning, the voltage is above 0 V, which corresponds to the formation in Li_xC_6 and Li–Ag alloy [47]. After that, there occurs a voltage plateau, which represents the metallic Li growth. SCT is the time when the voltage drastically changes to nearly 0 V and this point can be distinctly observed in the profile. We summarized the SCT data with upper and lower limits of Ag (B), bare CP and Ag (F) cells in Fig. 5B. Each group had at least three samples. Obviously, the Ag (B) cells have the longest SCT with a wide range: some SCTs can reach 2180 min, while others are close to those of bare CP. The reason is speculated that, in the current design, majority of the Li metal is deposited on the Ag side away from the Li counter electrode, whereas a small amount of the Li metal still on the carbon side. However, the SCT performance of Ag (B) is better than that of bare CP and Ag (F) as a result of controlled Li electrodeposition. For bare CP and Ag (F), they have stable short SCT because the primary deposition side is the surface facing the Li electrode. The Ag (F) cells have the shortest SCT because of the single side deposition, and this structure is harmful for the safety of the LIBs. In conclusion, the Li metal/carbon composite anode with the Ag (B) substrate is helpful to prevent the short-circuit from occurrence.

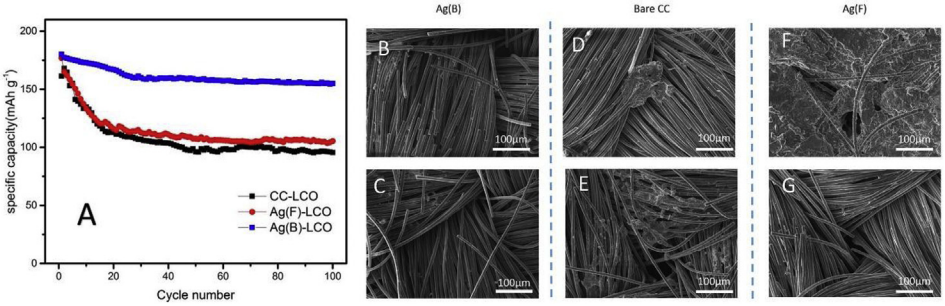

Fig. 7. Specific capacities of the full-cell tests (A). SEM images of the surfaces in the Ag (B) cells (B and C), bare CC cells (D and E) and Ag (F) cells (F and G) after 100 cycles. (A colour version of this figure can be viewed online.)

3.5. Coulombic efficiency tests

To evaluate the electrochemical performance of the composite anode, the CE test was carried out in ester-based electrolyte for the Ag (B), Ag (F) and bare CC cells. A specific current density of 1 mA cm^{-2} and a specific capacity of 5 mAh cm^{-2} were used in the galvanostatic charge/discharge tests. As shown in Fig. 6A, the CEs are about 98% in at the beginning. The CE cannot reach 100% as a result of the SEI and "dead Li" formation. Due to the poor electrical conductivity of an accumulated thick layer of SEI debris, once the root of lithium is stripped away during the stripping half-cycle, the remaining part of lithium may break off and lose its electrical connection to the electrode [48]. This process contributes to the "dead Li" formation and a poor Coulombic efficiency. After that, there are obvious CE drops in the three samples due to the explosive growth of dead Li. The Ag (F) CE quickly drops after 20 cycles, and that of the bare CC starts dropping after 25 cycles. By contrast, the Ag (B) CE drop does not occur till 32 cycles. This result indicates that the Ag (B) cell can restrain the "dead Li" formation and provide the best electrochemical stability (Fig. 6B).

In order to further analyze the reason, we took the SEM images (Fig. 6C–H) of the electrode after 40 cycles. The powdery "dead Li", which contributes to the serious CE drop, is discovered on the electrode. For Ag (B) (Fig. 6C and D), there are nearly equivalent amounts of "dead Li" on the two sides of the electrode. After considering the amounts of deposited Li on the two surfaces in Figs. S6A and B, we come to understand that "dead Li" is easy to form on the surface facing the Li counter electrode. The SEM images of bare CC (Fig. 6E and F) and Ag (F) (Fig. 6G and H) after cycling show that the carbon fibers are deeply embedded in the "dead Li" on the surface facing the Li counter electrode and only a little "dead Li" is on the back surface. Evidently, the CE differences are caused by the unique deposition behavior. Normally the growth direction of electrodeposited Li metal is towards the Li counter electrode. If the nucleation site is on the surface back to the Li counter electrode, the electrodeposited Li metal will grow into the CC, which can provide the electrical conduction during the subsequent stripping process. But if the nucleation site is on the front surface facing the Li counter electrode, the electrodeposited Li metal will grow toward the separator, which cannot provide the electrical conduction in the striping process (Fig. 6B). When Li loses electrical connection to the substrate, "dead Li" forms. When "dead Li" occupies most of the surface of the electrode (Fig. 6E and G), the following electrodeposited Li metal is hard to connect to CC and mostly forms "dead Li" in the striping process, resulting in the quick CE drop. Hence, the unique deposition direction in Ag (B) also provides better electrochemical performance in the CE tests.

3.6. Full cell tests

Lastly, we investigated the full-cell performance with the composite anodes. The Li metal/carbon composite anodes were prepared by electrochemically lithiating the modified CC electrodes to 2 mAh cm^{-2}. LCO cathode and ester-based electrolyte were employed to constitute the full cell. As shown in Fig. 7A, the three samples show similar first specific discharge capacities about 170 mAh g^{-1}. Afterwards, the capacity decay occurs because the "dead Li" formation consumes the limited Li element in the full cells [33]. After 100 cycles, the Ag (B) cell still remained a specific capacity of 155 mAh g^{-1}, which is distinctly higher than those of Ag (F) (105.4 mAh g^{-1}) and bare CC (95.6 mAh g^{-1}) (Figs. 7A and S10). From the SEM images (Fig. 7B–G) of the electrodes after 100 cycles, there is little "dead Li" on the Ag (B) electrode's surface, contributing to the best capacity retention. The presence of "dead Li" in the Ag (F) and bare CC electrode explains the reason of the serious capacity decay, which is consistent with the conclusion in the CE tests.

4. Conclusion

This work investigates the electrodeposition behavior of lithium metal on carbon substrates with surface silvering. We first employ the DFT calculation to analyze the absorption energy of Li atom on the surfaces of Li–Ag (100) and LiC_6 (001), and find that the preferential and uniform Li deposition may occur on the Li–Ag surface. Then the electrodeposition experiments show that surface silvering indeed can affect the deposition direction of Li metal on carbon substrates and restrain the formation of Li dendrites. Based on these, we examine the electrochemical performance of three types of Li metal/carbon composite anodes, namely, Ag (B), bare CP and Ag (F). The Ag (B) cells, benefiting from the suppression of "dead Li" formation, exhibit the longest short-circuit time, the highest Coulombic efficiency and the best capacity retention in the full cell tests. By correlating these basic results of the electrodeposition behavior and electrochemical performance, we give an elementary cognition of the influence of Li-alloyed surface and provide a guidance to construct the high-performance Li metal composite anodes.

Acknowledgements

This work is supported by the Joint Fund of Equipment Pre-Research and Ministry of Education of China (18GFA-ZZ07-172), Natural Science Foundation of China (no. 11304198) and Medical-Engineering Cross Fund of Shanghai Jiao Tong University (no. YG2017QN22). Instrumental Analysis Center of Shanghai Jiao Tong University, National Engineering Research Center for Nanotechnology, Prof. Liwei Chen's group, Mr. Feng Guo, and Mr. Hui Jiang of SINANO-CAS are gratefully acknowledged for assisting with relevant analyses.

Appendix A. Supplementary data

Supplementary data to this article can be found online at https://doi.org/10.1016/j.carbon.2019.06.067.

References

[1] V. Etacheri, R. Marom, R. Elazari, G. Salitra, D. Aurbach, Challenges in the development of advanced Li-ion batteries: a review, Energy Environ. Sci. 4 (9) (2011) 3243–3262.
[2] X.-B. Cheng, R. Zhang, C.-Z. Zhao, Q. Zhang, Toward safe lithium metal anode in rechargeable batteries: a review, Chem. Rev. 117 (15) (2017) 10403–10473.
[3] D. Lin, Y. Liu, Y. Cui, Reviving the lithium metal anode for high-energy batteries, Nat. Nanotechnol. 12 (2017) 194.
[4] W. Xu, J. Wang, F. Ding, X. Chen, E. Nasybulin, Y. Zhang, et al., Lithium metal anodes for rechargeable batteries, Energy Environ. Sci. 7 (2) (2014) 513–537.
[5] Y. Guo, H. Li, T. Zhai, Reviving lithium-metal anodes for next-generation high-energy batteries, Adv. Mater. 29 (29) (2017), 1700007.
[6] W. Liu, Y. Xia, W. Wang, Y. Wang, J. Jin, Y. Chen, et al., Pristine or highly defective? Understanding the role of graphene structure for stable lithium metal plating, Adv. Energy Mater. 9 (3) (2019), 1802918.
[7] P. Hundekar, S. Basu, J. Pan, S.F. Bartolucci, S. Narayanan, Z. Yang, et al., Exploiting self-heat in a lithium metal battery for dendrite healing, Energy Stor. Mater. (2019), https://doi.org/10.1016/j.ensm.2019.04.013 (in press).
[8] K.N. Wood, M. Noked, N.P. Dasgupta, Lithium metal anodes: toward an improved understanding of coupled morphological, electrochemical, and mechanical behavior, ACS Energy Lett 2 (3) (2017) 664–672.
[9] D. Lin, Y. Liu, A. Pei, Y. Cui, Nanoscale perspective: materials designs and understandings in lithium metal anodes, Nano Res 10 (12) (2017) 4003–4026.
[10] L. Li, S. Basu, Y. Wang, Z. Chen, P. Hundekar, B. Wang, et al., Self-heating–induced healing of lithium dendrites, Science 359 (6383) (2018) 1513.
[11] F. Ding, W. Xu, G.L. Graff, J. Zhang, M.L. Sushko, X. Chen, et al., Dendrite-free lithium deposition via self-healing electrostatic shield mechanism, J. Am. Chem. Soc. 135 (11) (2013) 4450–4456.
[12] X.-Q. Zhang, X. Chen, X.-B. Cheng, B.-Q. Li, X. Shen, C. Yan, et al., Highly stable

lithium metal batteries enabled by regulating the solvation of lithium ions in nonaqueous electrolytes, Angew. Chem. Int. Ed. 57 (19) (2018) 5301–5305.
[13] Y. Li, B. Xu, H. Xu, H. Duan, X. Lü, S. Xin, et al., Hybrid polymer/garnet electrolyte with a small interfacial resistance for lithium-ion batteries, Angew. Chem. Int. Ed. 56 (3) (2016) 753–756.
[14] D. Lin, Y. Liu, Z. Liang, H.-W. Lee, J. Sun, H. Wang, et al., Layered reduced graphene oxide with nanoscale interlayer gaps as a stable host for lithium metal anodes, Nat. Nanotechnol. 11 (2016) 626.
[15] A.C. Kozen, C.-F. Lin, A.J. Pearse, M.A. Schroeder, X. Han, L. Hu, et al., Next-generation lithium metal anode engineering via atomic layer deposition, ACS Nano 9 (6) (2015) 5884–5892.
[16] R. Tian, X. Feng, H. Duan, P. Zhang, H. Li, H. Liu, et al., Low-weight 3D Al2O3 network as an artificial layer to stabilize lithium deposition, ChemSusChem 11 (18) (2018) 3243–3252.
[17] H. Wu, Y. Cao, L. Geng, C. Wang, In situ formation of stable interfacial coating for high performance lithium metal anodes, Chem. Mater. 29 (8) (2017) 3572–3579.
[18] J. Xie, L. Liao, Y. Gong, Y. Li, F. Shi, A. Pei, et al., Stitching h-BN by atomic layer deposition of LiF as a stable interface for lithium metal anode, Sci. Adv. 3 (11) (2017), eaao3170.
[19] R. Zhang, X. Chen, X. Shen, X.-Q. Zhang, X.-R. Chen, X.-B. Cheng, et al., Coralloid carbon fiber-based composite lithium anode for robust lithium metal batteries, Joule 2 (4) (2018) 764–777.
[20] R. Tian, H. Duan, Y. Guo, H. Li, H. Liu, High-coulombic-efficiency carbon/Li clusters composite anode without precycling or prelithiation, Small 14 (33) (2018), 1802226.
[21] Y. Sun, G. Zheng, W. Seh Zhi, N. Liu, S. Wang, J. Sun, et al., Graphite-encapsulated Li-metal hybrid anodes for high-capacity Li batteries, Chem 1 (2) (2016) 287–297.
[22] R. Tian, S. Wan, L. Guan, H. Duan, Y. Guo, H. Li, et al., Oriented growth of Li metal for stable Li/carbon composite negative electrode, Electrochim. Acta 292 (2018) 227–233.
[23] G. Hou, X. Ren, X. Ma, L. Zhang, W. Zhai, Q. Ai, et al., Dendrite-free Li metal anode enabled by a 3D free-standing lithiophilic nitrogen-enriched carbon sponge, J. Power Sources 386 (2018) 77–84.
[24] H. Ye, S. Xin, Y.-X. Yin, J.-Y. Li, Y.-G. Guo, L.-J. Wan, Stable Li plating/stripping electrochemistry realized by a hybrid Li reservoir in spherical carbon granules with 3D conducting skeletons, J. Am. Chem. Soc. 139 (16) (2017) 5916–5922.
[25] C. Zhang, Z. Huang, W. Lv, Q. Yun, F. Kang, Q.-H. Yang, Carbon enables the practical use of lithium metal in a battery, Carbon 123 (2017) 744–755.
[26] S. Liu, X. Xia, Y. Zhong, S. Deng, Z. Yao, L. Zhang, et al., 3D TiC/C core/shell nanowire skeleton for dendrite-free and long-life lithium metal anode, Adv. Energy Mate. 8 (8) (2018), 1702322.
[27] R. Zhang, X.R. Chen, X. Chen, X.B. Cheng, X.Q. Zhang, C. Yan, et al., Lithiophilic sites in doped graphene guide uniform lithium nucleation for dendrite-free lithium metal anodes, Angew. Chem. Int. Ed. 56 (27) (2017) 7764–7768.
[28] Y. Wang, C.-Y. Wang, K.S. Chen, Elucidating differences between carbon paper and carbon cloth in polymer electrolyte fuel cells, Electrochim. Acta 52 (12) (2007) 3965–3975.
[29] H. Zhang, J. Yang, H. Hou, S. Chen, H. Yao, Nitrogen-doped carbon paper with 3D porous structure as a flexible free-standing anode for lithium-ion batteries, Sci. Rep. 7 (1) (2017) 7769.
[30] W. Ren, W. Ma, M.M. Umair, S. Zhang, B. Tang, CoO/Co-Activated porous carbon cloth cathode for high performance Li–S batteries, ChemSusChem 11 (16) (2018) 2695–2702.
[31] D. Huang, S. Li, X. Zhang, Y. Luo, J. Xiao, H. Chen, A novel method to significantly boost the electrocatalytic activity of carbon cloth for oxygen evolution reaction, Carbon 129 (2018) 468–475.
[32] C. Shen, G. Hu, L.-Z. Cheong, S. Huang, J.-G. Zhang, D. Wang, Direct observation of the growth of lithium dendrites on graphite anodes by operando EC-AFM, Small Methods 2 (2) (2018), 1700298.
[33] J. Qian, D. Adams Brian, J. Zheng, W. Xu, A. Henderson Wesley, J. Wang, et al., Anode-free rechargeable lithium metal batteries, Adv. Funct. Mater. 26 (39) (2016) 7094–7102.
[34] S.H. Wang, Y.X. Yin, T.T. Zuo, W. Dong, J.Y. Li, J.L. Shi, et al., Stable Li metal anodes via regulating lithium plating/stripping in vertically aligned microchannels, Adv. Mater. 29 (40) (2017), 1703729.
[35] G. Kresse, J. Furthmüller, Efficient iterative schemes for ab initio total-energy calculations using a plane-wave basis set, Phys. Rev. B 54 (16) (1996) 11169–11186.
[36] P.E. Blöchl, Projector augmented-wave method, Phys. Rev. B 50 (24) (1994) 17953–17979.
[37] J.P. Perdew, K. Burke, M. Ernzerhof, Generalized gradient approximation made simple, Phys. Rev. Lett. 77 (18) (1996) 3865–3868.
[38] G. Taillades, J. Sarradin, Silver: high performance anode for thin film lithium ion batteries, J. Power Sources 125 (2) (2004) 199–205.
[39] A.M. Shanmugharaj, S.H. Ryu, Excellent electrochemical performance of graphene-silver nanoparticle hybrids prepared using a microwave spark assistance process, Electrochim. Acta 74 (2012) 207–214.
[40] H. Zheng, K. Jiang, T. Abe, Z. Ogumi, Electrochemical intercalation of lithium into a natural graphite anode in quaternary ammonium-based ionic liquid electrolytes, Carbon 44 (2) (2006) 203–210.
[41] J. Lv, F. Lai, L. Lin, Y. Lin, Z. Huang, R. Chen, Thermal stability of Ag films in air prepared by thermal evaporation, Appl. Surf. Sci. 253 (17) (2007) 7036–7040.
[42] Y. Shao, H. Wang, Z. Gong, D. Wang, B. Zheng, J. Zhu, et al., Drawing a soft interface: an effective interfacial modification strategy for garnet-type solid-state Li batteries, ACS Energy Lett 3 (6) (2018) 1212–1218.
[43] Y. Zhou, C. Zhou, Q. Li, C. Yan, B. Han, K. Xia, et al., Enabling prominent high-rate and cycle performances in one lithium–sulfur battery: designing perm-selective gateways for Li^+ transportation in Holey-CNT/S cathodes, Adv. Mater. 27 (25) (2015) 3774–3781.
[44] Y. Wang, Y. Shen, Z. Du, X. Zhang, K. Wang, H. Zhang, et al., A lithium–carbon nanotube composite for stable lithium anodes, J. Mater. Chem. 5 (45) (2017) 23434–23439.
[45] F. Guo, Y. Wang, T. Kang, C. Liu, Y. Shen, W. Lu, et al., A Li-dual carbon composite as stable anode material for Li batteries, Energy Stor. Mater. 15 (2018) 116–123.
[46] Y. Lu, Z. Tu, L.A. Archer, Stable lithium electrodeposition in liquid and nanoporous solid electrolytes, Nat. Mater. 13 (2014) 961.
[47] K. Yan, Z. Lu, H.-W. Lee, F. Xiong, P.-C. Hsu, Y. Li, et al., Selective deposition and stable encapsulation of lithium through heterogeneous seeded growth, Nat. Energy. 1 (2016) 16010.
[48] J. Xie, J. Wang, H.R. Lee, K. Yan, Y. Li, F. Shi, et al., Engineering stable interfaces for three-dimensional lithium metal anodes, Sci. Adv. 4 (7) (2018).